PPPL-3186 - Preprint: May 1996, UC-420, 426, 427

Model of Alpha Particle Diffusion in the Outer Limiter Shadow of TFTR

Shaojie Wang* and S. J. Zweben

Princeton Plasma Physics Laboratory, P.O. Box 451, Princeton, New Jersey 08543

* Institute of Plasma Physics, Academia Sinica,

P. O. Box 1126, Hefei, Anhui, 230031, P. R. China

Abstract

A new code, Monte Carlo Collisional Stochastic Orbit Retracing (MCCSOR), has been developed to model the alpha particle loss signal as measured by the outer midplane scintillator detector in TFTR. The shadowing effects due to the outer limiters and the detector itself have been included, along with pitch angle scattering and stochastic ripple diffusion. Shadowing by the outer limiters has a strong effect on both the magnitude and pitch angle distribution of the calculated loss. There is at least qualitative agreement between the calculated results and the experimental data.

1. Introduction

The confinement of the energetic fusion product alpha particles is an important issue for the future D-T fusion reactors. Unanticipated alpha particle loss would not only degrade the alpha heating efficiency, but also might damage the first wall due to localized alpha particle energy loss. In addition to the usual first orbit loss, alpha particle diffusion is expected to be due to the periodic modulation of the toroidal magnetic field (TF). This Stochastic TF Ripple Diffusion (SRD) [1] is expected be much larger than first-orbit loss for high-current tokamak reactors like ITER [2]. Since Goldston, White and Boozer published their paper describing the first theoretical model for SRD [1], several detailed numerical calculations [for example Refs. 2-5] and experiments [for example Refs. 6-8] have been done to address this problem.

In order to test the GWB model with experiments, there should be a realistic numerical simulation of alpha loss. Recently, a set of alpha particle loss data has been acquired by the radially movable outer midplane scintillator detector mounted in TFTR [9]. It has been experimentally found that both the integrated alpha loss (per fusion reaction) and the pitch angle distribution of the alpha loss signal vary significantly during a major-radial scan of the midplane detector, as was also observed for D-D fusion product measurements using the same detector in TFTR [6,7]. For these radial scan experiments, the local shadowing effect of outer limiters and probe itself appears to be important, since these scans typical cover only a few centimeters around the geometrical "shadow" of the outer limiter edge. The existing numerical codes have generally not included these geometric shadowing effects, even though they can be important for determining the local alpha heat flux to the wall in the actual machines.

An earlier attempt to model these geometrical shadowing effects was done for the TFTR DD midplane detector experiments on fusion product ripple loss [7]. Those calculations for the limiter shadowing effect assumed a fixed particle diffusion rate, and compared the calculated radial fall-off with DD fusion product loss measurements. The best fit was obtained for a diffusion step size of 0.65 cm, which was close to the expected GWB step size of 0.75 cm. However, the expected signals were not calculated directly from the GWB model. In order to more directly compare the measured alpha loss signal with the GWB model, a new code, MCCSOR, was written to include these shadowing effect, as described below.

2. Geometry of the Detector and Limiters

The "midplane" lost alpha detector has a small aperture (≈0.1 cm x 0.2 cm) which can be scanned horizontally in the major radius direction at a fixed poloidal angle of ≈20° below the outer midplane, as illustrated in Fig. 1. The normal scan range is within a few cm of the geometrical "shadow" of the outer limiters, which are circular poloidal rings (Fig. 1a) located at various toroidal angles around the vessel (these are sometimes referred to as RF limiters, since they were designed to protect the RF antennas). The limiter nearest to the detector is about 45º toroidally in the direction of the alphas incident onto the detector (i.e. about 2 m toroidally) (Fig. 1b). There are a total of 9 limiters around the

vessel, with their inner edges defining a geometrical shadow with a major radius of R=260.6 cm and a minor radius of 99 cm (aligned to an accuracy of about 0.3 cm). Most of these limiters do not cover the complete poloidal circumference of the TFTR vessel, e.g. often leaving a gap within ±30° around the outer midplane. The toroidally symmetric solid outer wall is at a radius of approximately 110 cm.

The detector probe itself is housed in a protective cylindrical shield with a diameter of 6.4 cm, in which the aperture hole located 3 cm from its end [9]. Thus the aperture is always 3 cm behind the geometrical shadow of the detector tip. The detector cylinder occupies about 0.001 times the toroidal circumference of the torus at the radius of the aperture; thus the shadowing effect of the detector is small compared to the shadowing effect of the limiters, at least when the probe is within a few cm of the limiter edge.

In the radial scans analyzed for this study, the plasma had dimensions of R=252 cm and a=87 cm, and the probe was scanned so that its aperture moved within $r_{ap} = \pm 1.5$ cm of the geometrical shadow of the limiters (R_{lim}=260.6, a_{lim}=99 cm). In this configuration the probe tip was at least 16 cm from the edge of the plasma itself.

3. Basic Model

The present model considers three distinct mechanisms by which an alpha particle can be collected by the detector. The simplest is first-orbit loss, in which an alpha born on a large trapped orbit intersects a limiter on its first orbit [10]. The second is TF ripple loss, in which a confined trapped alpha banana tip diffuses vertically under the influence of SRD [1]. The third is a mechanism specific to this detector by which a normally *confined* alpha orbit can be detected if the aperture is located radially *inside* the geometrical shadow of the limiter. The latter mechanism is not relevant for the other alpha detectors in TFTR, which are located in the geometrical shadow of the limiter.

To strictly treat this problem a 3-D model should be used, but that would be intractable given the large number of orbits followed by our Monte Carlo technique. For the present study, we use a reduced 2-D model to consider the limiter shadowing effect. This reduction is accomplished by assuming that the toroidal angle of the particle's bounce orbit is random as it crosses the outer midplane. This assumption has been examined by numerical calculation [7], and is also corroborated by the fact the

toroidal procession frequency of alpha particle is much higher than its bounce frequency. For the standard case analyzed below, the probability for the particle to hit a limiter on each bounce, P_{lim}, is assumed be the fraction of the toroidal width of all the limiters with respect to the total circumference at the outboard wall. This ratio is estimated to be P_{lim}=0.075 for the TFTR limiter configuration, based on the fractional toroidal angle covered by the limiters near the outboard midplane, independent of the details of the alpha particle orbits. The validity of this assumption is discussed further in Sec. 6

With this assumption, the particle is launched from the detector and retraced backward in time. This orbit retracing technique is similar to that used in [7], and we adopt this technique to save computing time for a given Monte Carlo statistical error. The time step is chosen to be one bounce period. During each bounce period, the guiding center orbit is determined by two constants of motion [5], namely the magnetic momentum (μ) canonical toroidal momentum (P_ϕ):

$$\psi(R, Z) - R\chi V = P_\phi \qquad (1a)$$

$$V^2(1 - \chi^2)\, R/(R_0 B_0) = \mu \qquad (1b)$$

where $\chi = V_{||} / V$, $\psi = Ze\,\Psi / (2\pi m)$, V is the particle velocity, $\Psi = \Psi(R,Z)$ is the conventional poloidal flux. For this analysis, the magnetic flux surfaces are assumed to be concentric with a specified $q(r) = q(0)\,[1 + (r/a)^2]^{exp}$, where the parameters q(0)=1 and exp=2 are chosen to match the experiment.

With Eq. 1, the guiding center orbit is determined in the R-Ψ representation, and then the orbit is mapped into the conventional R-Z representation by $\Psi = \Psi(R,Z)$. From Eq. 1, one can see that for a given equilibrium configuration and a given velocity of the particle, the guiding center orbit of the particle is only determined by its three initial values χ_i , R_i and Z_i. Once the bounce orbit is determined, the contribution of this bounce period to the detected alpha particle signal f_α (normalized to the alpha source rate) is determined by integrating the alpha source along the orbit length elements "dl" [9]:

$$f_\alpha = \int S_\alpha dl \qquad (2)$$

After the outer midplane crossing point of each bounce, if $R_{ox} > R_w$ the retracing is stopped; here R_{ox} is the major radius of the outer midplane crossing point of the orbit, and r_w is the radius of the wall at the outer midplane. If $R_w > R_{ox} > R_{olim}$ the retracing is stopped with the probability of P_{lim}, where R_{olim} is the radius of the limiter at the outer midplane.

If the particle retracing procedure has not been stopped due to its hitting the first wall or the limiter, the next bounce period is calculated. For convenience of numerical calculation, although the initial value of (R_i, Z_i) for the first orbit is chosen to be the position of detector's aperture, the initial value of (R_i, Z_i) for the next orbit is chosen to be the banana tip (R_{tip}, Z_{tip}) of the preceding bounce orbit. At the start of the next bounce, collisional pitch angle scattering is applied to the particle. To model the pitch angle scattering effect, we randomly vary the χ_i according to

$$(\Delta\theta)^2 = (\pi / 2)^2 \nu_\perp \tau_b \qquad (3a)$$

$$\chi_i = \cos(\pi / 2 + \Delta\theta) \qquad (3b)$$

where $\nu_\perp$ is the conventional 90° collision frequency, τ_b is the bounce period (see Table I).

If the TF ripple strength δ at the banana tip satisfies the GWB stochasticity criterion [1]:

$$\delta > [\varepsilon / (Nq\pi)]^{1.5} / (\rho q') \qquad (4a)$$

where N is the number of TF coils (20), ρ is the alpha gyroradius and q and q' are calculated from the assumed profile, then the standard SRD model is applied to randomly vary the vertical coordinates of the banana tip according to:

$$\Delta Z = \delta\rho[Nq / (\varepsilon \sin \xi)]^{1.5} \qquad (4b)$$

where ξ is the poloidal angle of the banana tip [1].

With these new initial values the subsequent bounce orbit is determined by Eq. 1 and its contribution to the detector collection fraction is calculated by Eq. 2. The Monte Carlo guiding center bounce orbit retracing procedure continues until the particle hits on an obstacle (the first wall, the RF limiter or the detector itself), or the retracing time exceeds an assumed fraction of the alpha particle slowing-down time. For the standard modeling case below, this fraction was assumed to be 0.1, since the measured alpha loss signal was within about 10% of the alpha birth energy. This procedure gives an approximate calculation of the collisional SRD-induced loss.

4. Monte Carlo Technique

By the computation scheme described in Section 3, for each chosen initial condition about 5000 particles were launched from the detector into the plasma. The resulting detector collection fraction was obtained with reasonable small statistical error (<5%) induced by the Monte Carlo method.

In our computing scheme, there are two steps involving Monte Carlo method: randomly changing the particle's magnetic moment by pitch angle scattering, and randomly determining if the particle hits the limiter (through P_{lim}). In order to obtain better statistical accuracy for a given number of sampling particles, a special weighting technique is employed. For the first bounce period, the weight of the particle is assigned to be 1. For the subsequent bounce periods which satisfy $R_W > R_{ox} > $ 'olim, we reduce the weight of the particle by the factor of $(1 - P_{lim})$, instead of simply randomly stopping the retracing procedure by the probability of P_{lim}. If the weight of the particle has been reduced to a given critical value W_{cr}, we resume the random stopping scheme to avoid trivial further computation. By this technique, the Monte Carlo statistical error is greatly reduced. With the same condition as calculated by the simple scheme mentioned above, this weighting technique reduces the number of particles needed to launch from 5000 to 2000 (the corresponding CPU time is reduced about 20%, and at the same time the statistic error is reduced from 5% to 3%.

5. Calculation Results and Comparison with Experiment

Calculations were done to compare this model with the D-T experimental results described in Ref. 9, with plasma, machine, and alpha particle parameters shown in Table 1. The code was used to

calculate the expected pitch angle distributions for various assumed detector aperture locations with respect to the outer limiter shadow. The resulting calculated pitch angle (ϑ) distributions are shown in Figs. 2 for the "standard case" with the parameters of Table 1. Note that these pitch angles (ϑ) are measured with respect to the local total magnetic field.

The limiter shadowing effect can be seen in Fig. 2 in the variation of the pitch angle distribution with respect to the assumed radial location of the detector aperture with respect to the edge of the limiter. When the aperture is well inside the limiter radius, e.g. r_{ap} = -1.5 cm, there is a large sharp component at a pitch angle $\vartheta \approx 50°$ which is strongly diminished as the detector is moved outward, i.e. toward r_{ap} = +2.5. There is also a broader distribution between $\vartheta \approx 53\text{-}68°$ which diminishes as it systematically shifts to higher pitch angles as the probe is moved outward.

The sensitivity of these results to various assumptions of the code are explored in Figs. 3-6. Fig. 3 shows the effect of turning off the collisional SRD-induced transport (i.e. setting δ= 0). The sharp peaks at $\vartheta \approx 50°$ remains, but the broad feature at $\vartheta \approx 53\text{-}68°$ disappears. Thus the broad feature at $\vartheta \approx 53\text{-}68°$ is due to SRD; this is consistent with previous calculations using the MAPLOS code [6]. Fig. 3 also shows that the sharp peak at $\vartheta \approx 50°$ remains after collisional SRD is turned off. This pitch angle is near the fattest banana orbit at this detector location; i.e. just below this angle there are confined passing alpha particles orbits. Therefore the large increase inside r_{ap}=0 is due to the collection of normally confined orbits, while the loss for r_{ap} >0 is due to first-orbit loss. The first-orbit loss is approximately independent of the radial position of the detector over this range, as expected.

Fig. 4 shows the results for the same parameters as Fig. 2, except that the detector self-shadowing probability parameter was increased from its standard value of P_{det} = 0.001 to P_{det} = 0.005. The increased self-shadowing caused a decrease in the sharp feature at $\vartheta \approx 50°$ due to an increase in the probability that the normally confined alpha particle will hit the probe before it is collected by the small aperture.

Fig. 5 shows the results for the same parameters as for Fig. 2, except that the orbits are followed for a period of f_{tran}=0.2 times the alpha energy e-folding time, instead of the f_{tran} =0.1 assumed for the standard case. The increased integration time causes a factor of two increase in the level of the collisional SRD feature at $\vartheta \approx 53\text{-}68°$. Evidently there is a component of the collisional TF ripple loss which

continues on a time scale comparable to the alpha particle slowing-down time; this is consistent with collisional guiding center calculations made using the ORBIT code [4].

Fig. 6 shows the results for the same parameters as Fig. 2, except that the RF limiter shadowing probability parameter was increased from its standard value of $P_{lim} = 0.075$ to $P_{lim} = 0.2$. The characteristic of the pitch angle distribution of Fig. 6 is similar to Fig. 2, but there is a more rapid decrease of the total loss signal as the detector is moved outward, due to the increased the probability of hitting the limiter (see Sec. 6).

The experimental pitch angle (ϑ_{Exp}) distributions for three aperture positions in this scan are shown in Fig. 7, for the same discharges described in Ref. [9]. Note that these pitch angles (ϑ_{Exp}) are shown with respect to the total magnetic field (as are the calculated pitch angles). As the detector is moved inward past the outer limiter shadow, the pitch angle (ϑ_{Exp}) distribution peaks toward a sharp feature near $\vartheta_{Exp} \approx 55°$, and as it moves outward into the limiter shadow, the pitch angle (ϑ_{Exp}) distribution broadens and peaks nearer $\vartheta_{Exp} \approx 66°$. The behavior of the measured pitch angle distributions are at least qualitatively similar to that predicted in the model calculations for the standard case in Fig. 2.

The total alpha particle loss (integrated over pitch angle) vs. aperture position is shown for both the measurements and the model calculations in Fig. 8. The measured alpha loss decreases by a factor of 20 over the radial range ±1.7 cm around the edge of the limiter shadow; however, the calculated loss based on the standard model (with $P_{lim}=0.075$) decreases by only about a factor of 4. For comparison, the model calculations without limiters ($P_{lim}=0$) and with a larger probability for hitting the limiters ($P_{lim}=0.2$) are also shown in this figure; evidently the case with $P_{lim}=0.2$ fits the data better.

6. Discussion

This model for the effect of the outer limiter shadowing on alpha detection near the outer midplane agreed at least qualitatively with the experimental data from TFTR. It correctly predicts the change in the shape of the detected alpha pitch angle distribution as the detector is moved radially in the range ±1.5 cm around the edge of the outer limiter shadow (comparing Fig. 2 with Fig. 7). The standard model also predicts a large decrease in total signal as the detector is moved behind the limiter

shadow, although not as large a decrease as observed experimentally (Fig. 8).

The mean pitch angle of the calculated alpha loss increases when the detector aperture moves outward due to the limiter shadowing effect. One cause for this is the collection of otherwise confined barely trapped orbits (with a small pitch angle $\vartheta \approx 50°$) when the aperture is moved more than about 1 cm inside the limiter shadow ($r_{ap} < -1$ cm). The other cause for this change in the pitch angle distribution vs. aperture position is the increase in the SRD radial step size with increasing pitch angle, caused by the increasing minor radius and ripple strength at the banana tip location. The higher the SRD-induced step size, the higher the probability for the particle to be detected far behind the limiter shadow. Conversely, because the barely trapped particles are marginally stochastic, they have a low diffusion rate and hence are quickly scraped off by the limiter as the detector is moved outward.

To understand the variation of the total loss vs. detector position, a simple analytical model can be used to evaluate the RF limiter shadowing effect. Assume that the alpha particle flux inside the RF limiters is I_0, and the aperture of the detector is located a distance "x" outside the RF limiters. The total loss of alpha particle collected by the aperture is assumed to be proportional to the alpha particle flux at x. Assuming that at every bounce the particles (mainly trapped) walk randomly with a step-size of Δb, and that they will be scraped-off by the RF limiters with a probability of P_{lim}, the total loss of alpha particle collected by the detector at x is proportional to $I(x)=I_0(1-P_{lim})^N$, where $N=x^2/\Delta b^2$ is the number of bounces needed for the particle to arrive at the aperture of the detector, as evaluated by a random walk model. For the standard case mentioned above, the average step size induced by SRD is about 0.5 cm, so about 9 bounces are needed for the alpha particle to randomly walk across the RF limiter shadowing region from x=0 to the aperture at x=1.5 cm. Therefore the expected variation of the total loss vs. detector position between x=0 and x=1.5 cm is about $(1-0.075)^9 \approx 0.5$, which agrees reasonably well with the results from MCCSOR code. From this simple analytical model, one can see that the variation of the total alpha loss vs. the radial position of the detector is sensitive to the probability, P_{lim}. Hence in order to obtain better comparison with the experiments, it is necessary to reexamine the evaluation of the parameter, P_{lim}.

As the end of this paper, we would like to make some general comments on evaluating the shadowing probability, P_{lim}, of the limiters. The estimate of $P_{lim}=0.075$ used for the standard case

was based on the simple geometrical fraction of the toroidal angle covered by limiters in TFTR (see Sec. 3). This was motivated by our 2-D model, which considered only the space-time evolution of the banana tip position in the poloidal plane. However, for the real 3-D bounce orbits, the evaluation of P_{lim} must also depend on the fraction of time the orbit spends in the limiter shadow, which in turn depends on the shape of the orbit itself. Thus the 3-D evaluation implies that P_{lim} is also a function of the orbit shape, and not a simple geometrical constant.

Noting that $\phi=q\xi$, (here ϕ is the toroidal angle and ξ is the poloidal angle), if the poloidal angle of the orbit behind the RF limiters shadow is assumed to be $\Delta\xi$, toroidally there should be a part $\Delta\phi=q\Delta\xi$ of the orbit falling into the shadowing region, implying a shadowing probability of $P_{orb}\approx\Delta\phi/2\pi$, roughly independent of the details of the limiter configuration. If $\Delta\xi$ is large enough, the value of P_{lim} (evaluated in Section 3) should be replaced by P_{orb}. Typical orbits entering the TFTR midplane probe aperture within the range $r_{ap}=\pm1.5$ cm have $\Delta\xi\approx30°$, implying that $P_{orb}>>P_{lim}$. However, a detailed calculation of P_{orb} would also depend on the complicated of the outer limiter structure near the midplane. For comparison purposes, the effect of assuming $P_{lim}=0.2$ on the radial profile to total loss is shown in Fig. 8, and this assumption fits the experiments better than $P_{lim}=0.075$. Thus it is likely that a 3-D model incorporating a self-consistent calculation of P_{lim} will be necessary to improve the fit to the experimental data. At the same time, a more accurate equilibrium (including the Shafranov shift), and the finite Larmor radius effect should also be included in future modeling.

Acknowledgments: We thank D. Darrow and H. Herrmann for discussions about the detector and orbit geometry. One of us (S. Wang) thanks R. White and K. McGuire for valuable discussions during his visit to PPPL. This work was done under Contract DE-AC02-76CH0-3073.

References

[1] R. J. Goldston, R. B. White, A. H. Boozer, Phys. Rev. Letts. **47**, 647 (1981)

[2] M. Redi, et al, PPPL-3171 submitted to Nuclear Fusion (1996)

[3] R. B. White, H. E. Mynick, Phys. Fluids B **1** (5), 980 (1989)

[4] M. H. Redi, R. Budny, D. Darrow, et al, Nucl. Fusion **35**, 1509 (1996)

[5] S. V. Putvinskii, Alpha Particles in Tokamaks, in Reviews of Plasma Physics, Vol. 18, edited by B. B. Kadomtsev, Consultants Bureau,New York, 1993

[6] R. L. Boivin, S. J. Zweben, R. B. White, Nuclear Fusion, **33**, 449 (1993)

[7] R. L. Boivin, S. J. Zweben, Phys. Fluids B **5** (5), 1559 (1993)

[8] K. Tobita, K. Tani, Y. Kusama, et al. , Nucl. Fus. **35**, 1585 (1996)

[9] S. J. Zweben, D. S. Darrow, H. W. Herrmann, et al, Nucl. Fus. **35**, 1445 (1995)

[10] S. J. Zweben, D. S. Darrow, H. W. Herrmann, et al, Nucl. Fus. **35**, 893 (1995)

Table 1 - Model Parameters for Standard Case

Plasma:

$R = 252$ cm

$a = 87$ cm

$I = 2.0$ MA

$B = 4.7$ T.

$q(r) = q(0)\,[1+(r/a)^2]^2$

$n = 3.3 \times 10^{13}$ cm^{-3}

$T_e = 7$ keV

Machine Geometry:

r_w = 110 cm (wall minor radius), centered at R_{lim}=260.6 cm

r_{lim} = 99 cm (limiter minor radius), centered at R_{lim}=260.6 cm

P_{lim} = 0.075

P_{det} = 0.001

Alpha particle parameters:

E= 3.5 MeV

ρ = 5 cm (at the magnetic axis)

bounce time $\tau_b = 2x10^{-5}$ sec

pitch angle scattering time $\tau_\perp$ =8.3 sec

energy e-folding time τ_α = 0.25 sec

fraction of orbit followed $f_{tran} = 0.1\ \tau_\alpha$

Figure Captions

Fig. 1 - Schematic picture of the detector geometry and the RF limiter shadowing effect showing (a) minor cross-section, and (b) midplane major cross-section. The detector aperture moves in the range ±1.5 cm with respect to the geometrical shadow of the poloidal limiters. Only a few of the 9 limiters are shown; most of these expend only partially around the poloidal cross section, but all have a common limiter edge at R_{lim}=260.6 cm and a_{lim}=0.99 cm.

Fig. 2 - Calculated pitch angle (ϑ) distribution of alpha loss signal for different positions of detector aperture (standard case). The curves correspond to aperture position of -1.5 cm (top), -0.5 cm, +0.5 cm, +1.5 cm and +2.5 cm (bottom), in that order. The expected alpha loss signal decreases as the aperture is moved behind the limiter shadow, while the mean pitch angle increases.

Fig. 3 - Effect of turning-off the stochastic TF ripple diffusion on the calculated pitch angle distribution of the alpha loss signal (comparing to the standard case). Turning off SRD leaves the first-orbit loss at $r_{ap}>0$, plus a contribution from normally confined non-diffusing orbits for $r_{ap} < 0$. The curves correspond to aperture position of -1.5 cm (top), -0.5 cm, +0.5 cm, +1.5 cm and +2.5 cm (bottom), in that order.

Fig. 4 - Effect of increasing the detector self-shadowing probability P_{det}=0.005 from P_{det}=0.001 to P_{det}=0.005 on the calculated pitch angle distribution of the alpha loss signal for the standard case. The increased detector shadowing reduces the collection of normally confined orbits at $r_{ap} < 0$, but does not significantly affect the collection of SRD-induced signal. The curves correspond to aperture position of -1.5 cm (top), -0.5 cm, +0.5 cm, +1.5 cm and +2.5 cm (bottom), in that order.

Fig. 5 - Effect of increasing the orbit retracing time to from f_{tran}=0.1 τ_α to f_{tran}=0.2 τ_α on the calculated pitch angle distribution of the alpha loss signal for the standard case. The increased retracing time increases the magnitude of the SRD-induced signal with respect to the first-orbit and normally confined orbit contributions. The curves correspond to aperture position of -1.5 cm (top), -0.5 cm, +0.5 cm, +1.5 cm and +2.5 cm (bottom), in that order.

Fig. 6 Effect of increasing the RF limiter shadowing probability from P_{lim}=0.075 to P_{lim}=0.2 on the calculated pitch angle distribution of the alpha loss signal for the standard case. The increase of P_{lim} causes a more rapid decrease of the calculated alpha signal behind the limiter shadow (also shown in Fig. 8). The curves correspond to aperture position of -1.5 cm (top), -0.5 cm, +0.5 cm, +1.5 cm and +2.5 cm (bottom), in that order.

Fig. 7 Measured pitch angle ϑ_{Exp} distribution of alpha loss with respect to the total magnetic field at the detector for three different aperture positions [9]. The mean pitch angle increases with increasing r_{ap}, at least qualitatively consistent with the modeling in Figs. 2-6. The vertical scale is the relative alpha signal per DT neutron, but the horizontal scale is absolutely calibrated to within about ±3°.

Fig. 8 Comparison of the calculation results and the experiment data for the integrated alpha loss (per neutron) vs. the radial position of the detector aperture. The models are all normalized to the data at r_{ap} = -1.5 cm, and assume various limiter hitting probabilities, with the best fit coming for P_{lim}=0.2. The decrease vs. aperture position for P_{lim}=0 is due to the detector self-shadowing.

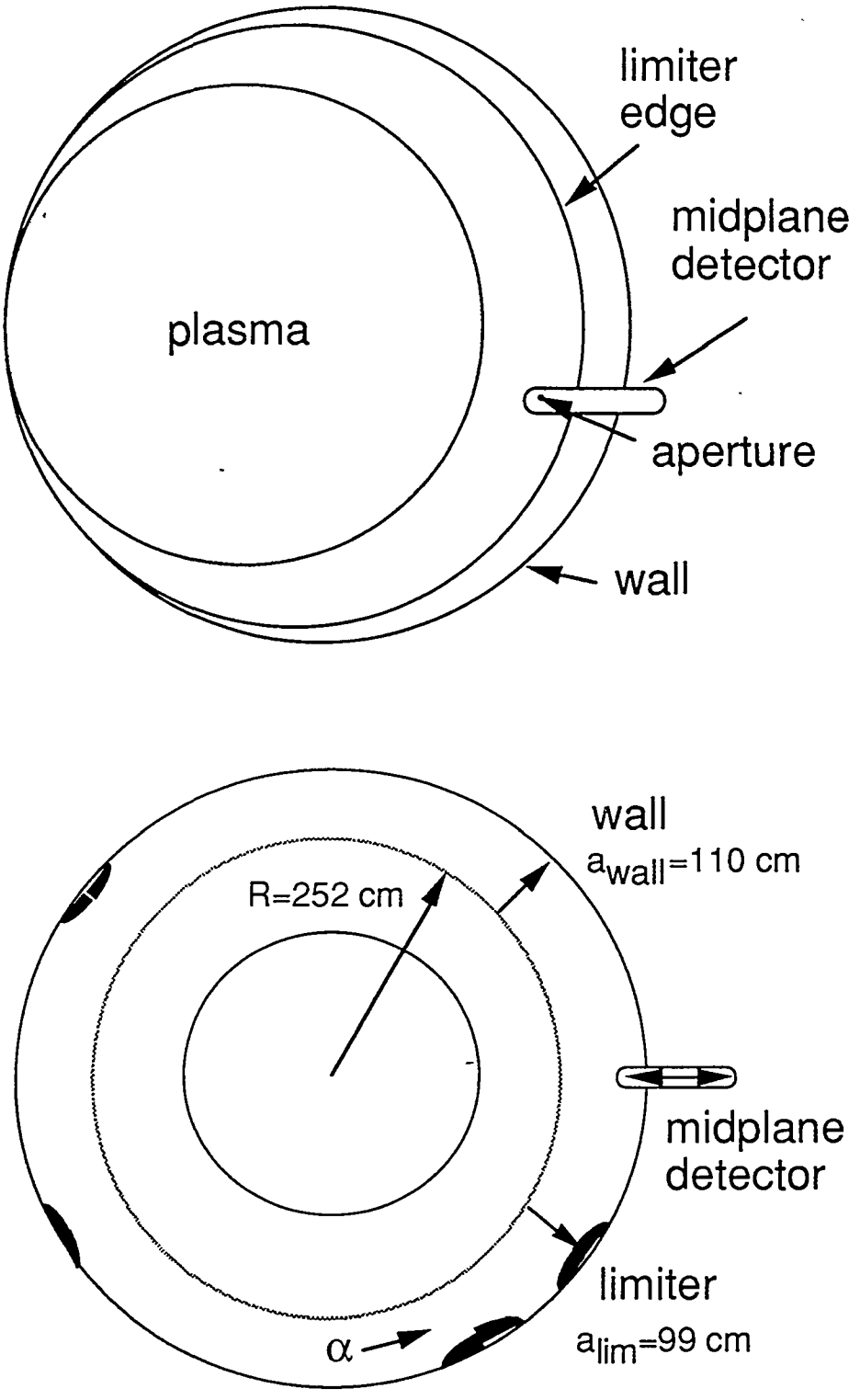
limiter
edge
midplane
detector
plasma
aperture
wall
wall
a_{wall}=110 cm
R=252 cm
midplane
detector
limiter
a_{lim}=99 cm
α

Fig. 1

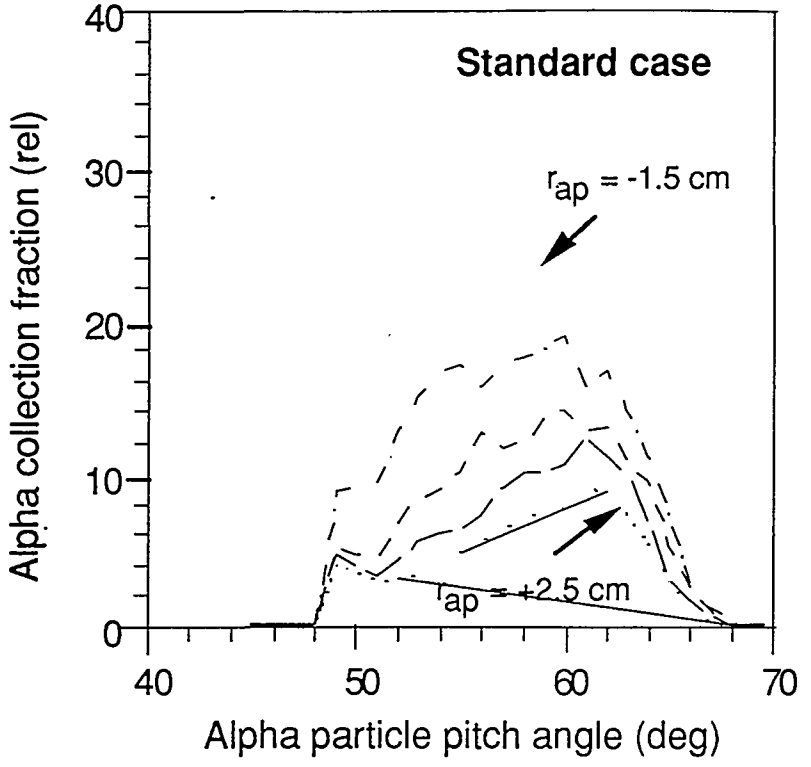
Standard case
r_{ap} = -1.5 cm
r_{ap} = +2.5 cm
Alpha collection fraction (rel)
Alpha particle pitch angle (deg)
0
10
20
30
40
40
50
60
70

Fig. 2

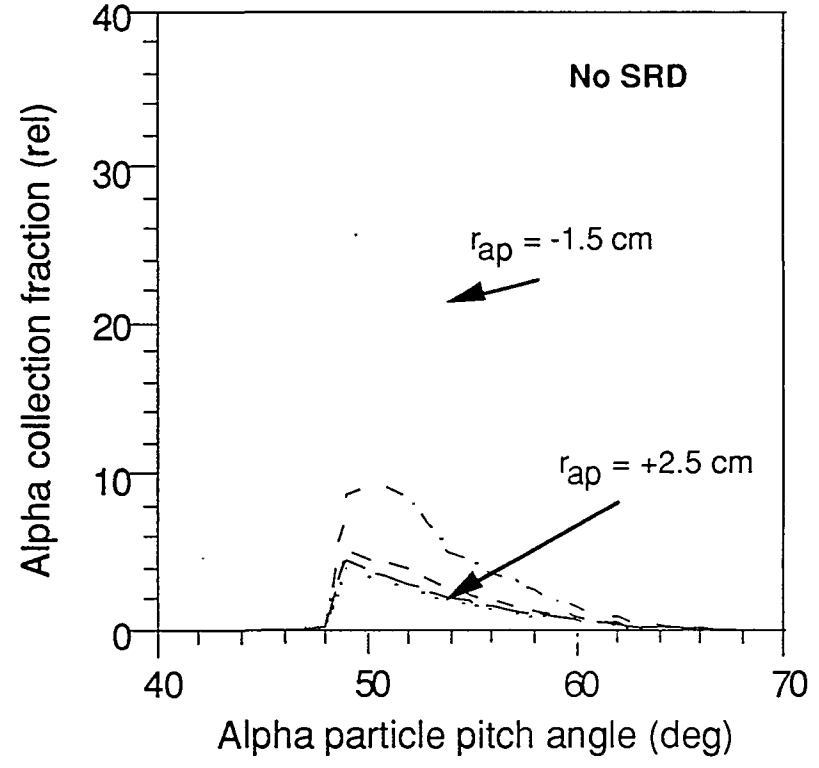
No SRD
r_{ap} = -1.5 cm
r_{ap} = +2.5 cm
Alpha collection fraction (rel)
Alpha particle pitch angle (deg)
0
10
20
30
40
40
50
60
70

Fig. 3

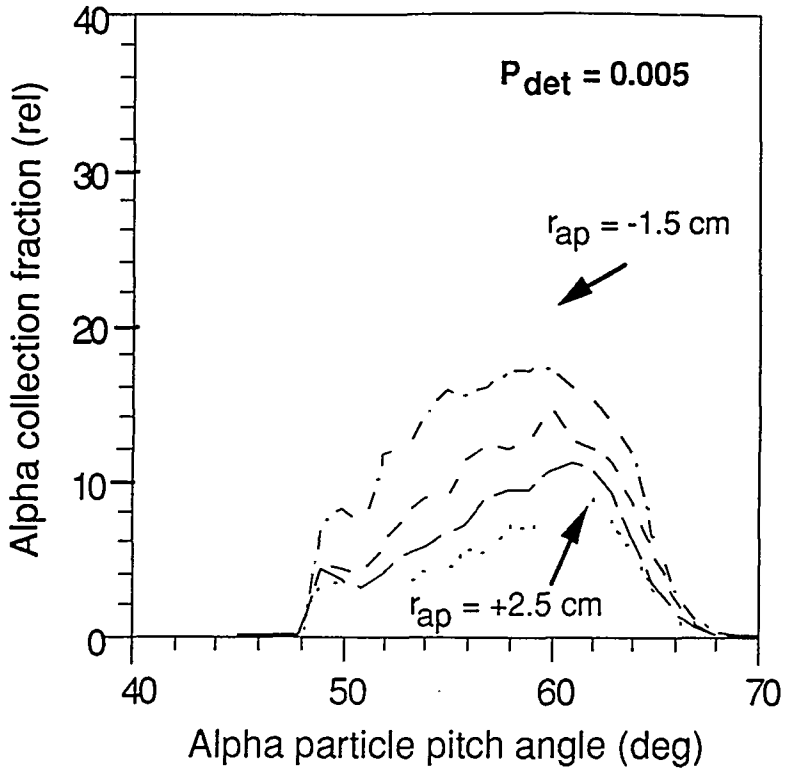
P_{det} = 0.005
r_{ap} = -1.5 cm
r_{ap} = +2.5 cm
Alpha collection fraction (rel)
Alpha particle pitch angle (deg)
0
10
20
30
40
40
50
60
70

Fig. 4

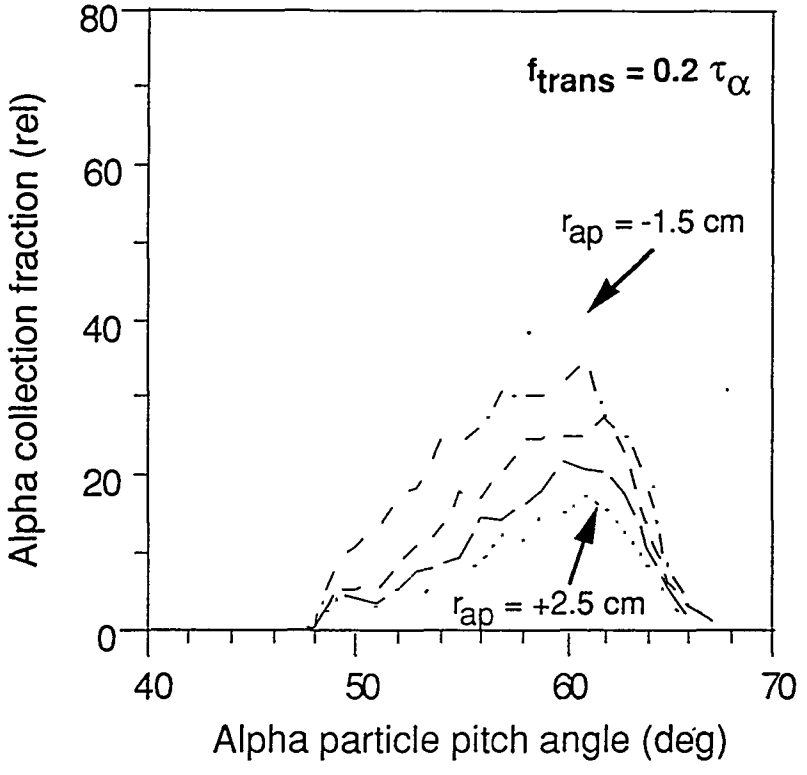
f_{trans} = 0.2 τ_α
r_{ap} = -1.5 cm
r_{ap} = +2.5 cm
Alpha collection fraction (rel)
Alpha particle pitch angle (deg)
0
20
40
60
80
40
50
60
70

Fig. 5

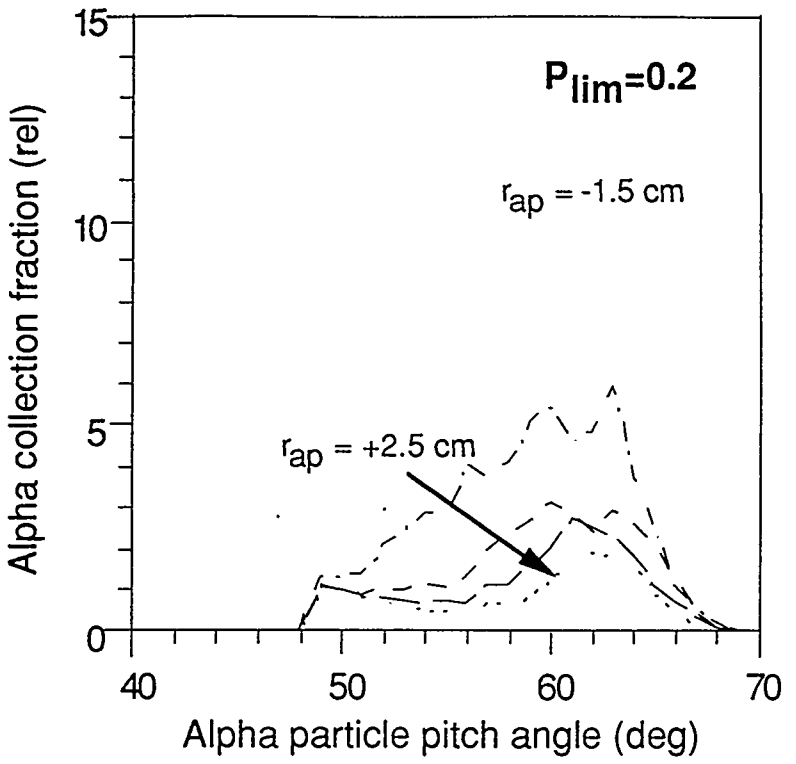
15
10
5
0
Alpha collection fraction (rel)
P_{lim}=0.2
r_{ap} = -1.5 cm
r_{ap} = +2.5 cm
40
50
60
70
Alpha particle pitch angle (deg)

Fig. 6

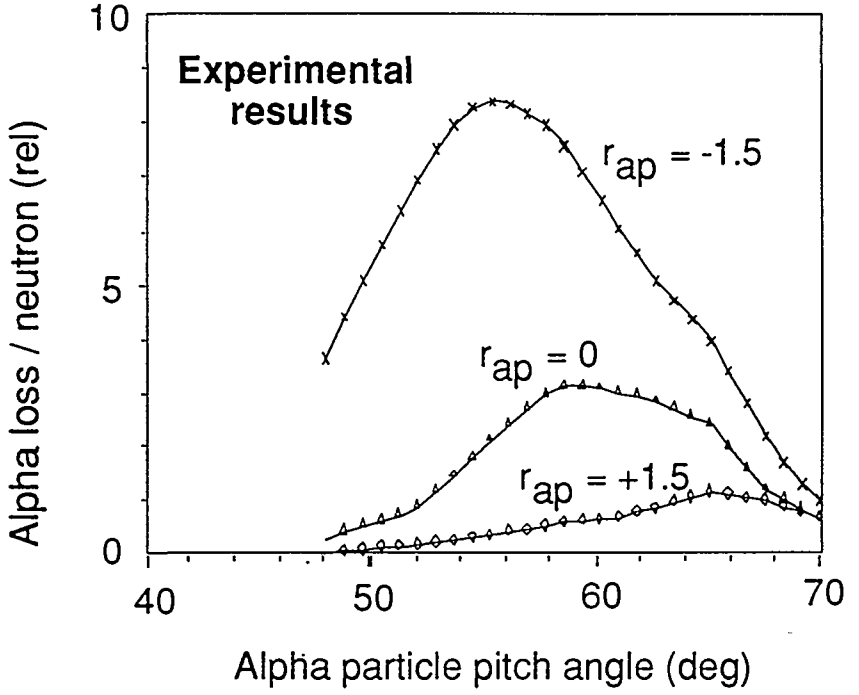
10
5
0
Alpha loss / neutron (rel)
Experimental results
r_{ap} = -1.5
r_{ap} = 0
r_{ap} = +1.5
40
50
60
70
Alpha particle pitch angle (deg)

Fig. 7

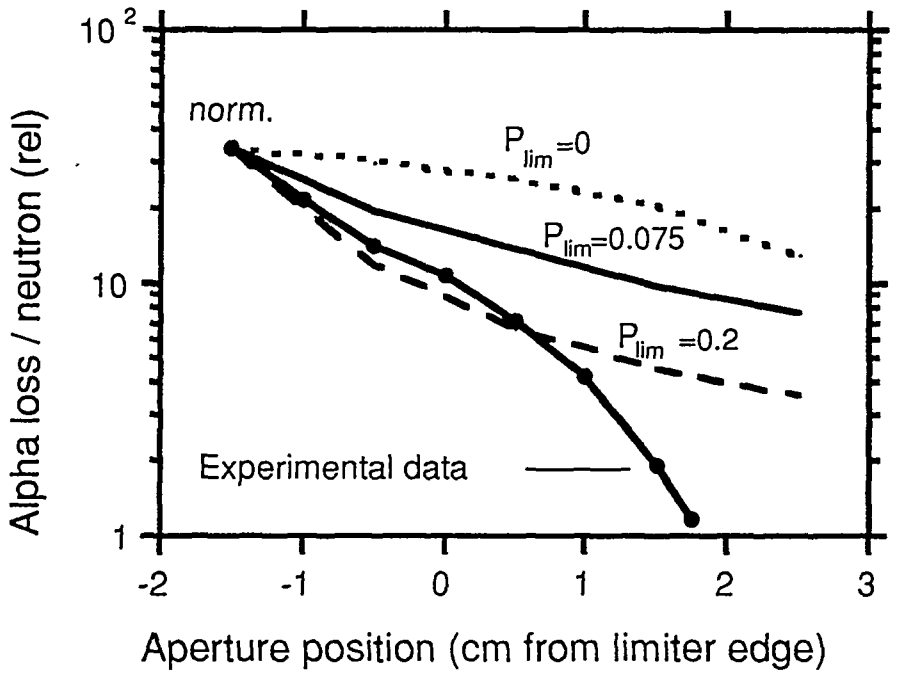

Fig. 8

DISCLAIMER